Geophysical Research Letters

RESEARCH LETTER
10.1029/2024GL111812

Secondary Reconnection Between Interlinked Flux Tubes Driven by Magnetic Reconnection With a Short X-Line

Kai Huang[1,2], Quanming Lu[3,4,5], Yi-Hsin Liu[6], San Lu[3,4,5], Xinmin Li[3,4,5], Huibo Tang[1,2], and E. Peng[2]

[1]School of Physics, Harbin Institute of Technology, Harbin, China, [2]Laboratory for Space Environment and Physical Sciences, Harbin Institute of Technology, Harbin, China, [3]Deep Space Exploration Laboratory/School of Earth and Space Sciences, University of Science and Technology of China, Hefei, China, [4]CAS Center for Excellence in Comparative Planetology/CAS Key Lab of Geospace Environment, University of Science and Technology of China, Hefei, China, [5]Collaborative Innovation Center of Astronautical Science and Technology, Harbin, China, [6]Department of Physics and Astronomy, Dartmouth College, Hanover, NH, USA

Key Points:

- Interlinked flux tubes can form during multiple x-line guide field reconnection when the x-line is short
- Secondary reconnection can be triggered in the current sheet formed between interlinked flux tubes
- The upstream magnetic field pileup is caused by the magnetic tension force

Correspondence to:
Q. Lu,
qmlu@ustc.edu.cn

Citation:
Huang, K., Lu, Q., Liu, Y.-H., Lu, S., Li, X., Tang, H., & Peng, E. (2024). Secondary reconnection between interlinked flux tubes driven by magnetic reconnection with a short x-line. *Geophysical Research Letters*, *51*, e2024GL111812. https://doi.org/10.1029/2024GL111812

Received 6 AUG 2024
Accepted 18 NOV 2024

Abstract

A three-dimensional particle-in-cell simulation is performed to study secondary reconnection between two interlinked flux tubes produced by neighboring guide field reconnection x-lines. The reconnecting magnetic fields of this secondary reconnection is enhanced toward the diffusion region, agree well with that in observations. The magnetic field pileup is attributed to the upstream magnetic tension force, that smashes the flux tubes into each other. We propose that the primary reconnection x-line length is a key parameter to determine the formation of interlinked flux tubes and secondary reconnection therein. Interlinked flux tubes will form only if the x-line is short; when the x-line is long enough, the regular flux ropes are formed instead. The critical x-line length to form interlinked flux tubes is determined by the distance between two neighbor x-lines and the magnetic shear angle of the primary reconnection. The results provide a novel scenario of secondary reconnection generation during three-dimensional reconnection.

Plain Language Summary

Magnetic reconnection is a fundamental energy conversion process in plasmas, and exists in varieties of space environments. Recent observations find magnetic reconnection occurring in the current sheet between two elbow like flux tubes interlinked with each other. The observational features of such a kind of event are very similar to that of a flux rope, which is a helical magnetic field structure. However, the formation condition for interlinked flux tubes and magnetic reconnection between them is not well understood, the relation between interlinked flux tubes and flux ropes is also not very clear. In this letter, we use three-dimensional particle-in-cell simulation to study the formation of magnetic reconnection between interlinked flux tubes, and propose an explanation for its formation.

1. Introduction

Magnetic reconnection converts magnetic energy into plasma kinetic and thermal energy by rearranging the magnetic connectivity, and is believed to be responsible for explosive phenomena in space environments, such as solar flares, coronal mass ejections (CMEs), and magnetospheric substorms (Angelopoulos et al., 2008; Lu et al., 2022; Masuda et al., 1994; Sergeev et al., 2012; Shibata et al., 1995). Recent studies also found that reconnection occurring on planets can enhance the ion escape and therefore may play an important role during the evolution of planets' atmosphere (Chen et al., 2023; L. Wang et al., 2023; L. Wang et al., 2022; T. L. Zhang et al., 2012). Besides large-scale current sheets like Earth's magnetopause and magnetotail current sheets, reconnection can also occur inside kinetic-scale current sheets generated by the earlier magnetic reconnection. Such a kind of reconnection is referred to as secondary reconnection. It can occur in the reconnection diffusion region (Daughton et al., 2006; Drake et al., 2006; Fermo et al., 2012; R. Wang et al., 2010; R. Wang et al., 2015; Z. H. Zhong et al., 2018), in the separatrix region (Daughton et al., 2011; K. Huang et al., 2022; S. Y. Huang et al., 2016), in the outflow region (C. Huang et al., 2015; Lapenta et al., 2022), at the reconnection fronts (Lapenta et al., 2015), and inside flux ropes (C. Huang et al., 2017; Lu et al., 2023; S. Wang et al., 2020).

Interlinked flux tubes are two elbowlike flux tubes interlinked with each other, and there is no magnetic connectivity between them. They are typical magnetic structures observed at magnetopause (Cardoso et al., 2013; Hesse et al., 1990; Kan, 1988; Lee et al., 1993; Louarn et al., 2004; Otto, 1995). They may form through random patchy reconnection, multiple x-line reconnection due to the accumulation of interplanetary magnetic field (IMF), the evolution of a flux rope into more complex 3D structures, or the bifurcated reconnection x-line (Fargette et al., 2020; Farinas Perez et al., 2018; Nishida, 1989). Recent observations at magnetopause showed that magnetic reconnection occurs between two interlinked flux tubes which are thought to originate from two reconnecting x-lines (Fargette et al., 2020; Kacem et al., 2018; Maheshwari et al., 2022; Øieroset et al., 2016, 2019). However, little was known about the condition for interlinked flux tubes as well as magnetic reconnection between them to form. Interlinked flux tubes have observational features similar to a flux rope, which has a bipolar variation of the magnetic field component in the normal direction of the current sheet and a strong core field along its axis (Russell & Elphic, 1978). However, their magnetic geometries are completely different. Flux ropes are helical magnetic field structures, while interlinked flux tubes have no internal twist. The relation between these two structures is far less understood.

Using a three-dimensional (3D) particle-in-cell (PIC) simulation, we show that secondary reconnection develops between interlinked flux tubes generated by neighboring short x-lines of guide field reconnection. We propose the detailed condition for the generation of interlinked flux tubes and explain the upstream flux pileup of reconnection between them. We also compare the differences between the generation of two interlinked flux tubes and a flux rope, and explain why secondary reconnection with upstream flux pileup may not occur inside a flux rope.

2. Simulation Model

The simulation is performed using the open-source 3D PIC code VPIC, which has been successfully used to numerically study plasma physics (Bowers, Albright, Bergen, et al., 2008; Bowers, Albright, Yin, et al., 2008; Bowers et al., 2009). The simulation set up is similar to that in K. Huang et al. (2023). The initial configuration is a Harris sheet with magnetic field $\boldsymbol{B}(z) = B_0 \tanh(z/\delta)\boldsymbol{e}_x + B_g\boldsymbol{e}_y$ and plasma density $n(z) = n_0 \operatorname{sech}^2(z/\delta) + n_b$. Here, B_0 is the asymptotic magnetic field, $B_g = B_0$ is the guide field, δ is the half-thickness of the current sheet, n_0 is the peak density of the current sheet, $n_b = 0.05n_0$ is the background density. The initial distributions of ions and electrons are Maxwellian while the current sheet populations have drift velocities along the y direction with $-V_{iy0}/V_{ey0} = T_{i0}/T_{e0} = 5$ to satisfy the Ampere's law $\nabla \times B = \mu_0 J$. Ion to electron mass ratio is set to be $m_i/m_e = 100$. The light speed is $c = 20V_A$, where V_A is the Alfvén speed defined by $V_A = B_0/\sqrt{\mu_0 n_0 m_i}$. The simulation domain is centered at $x = y = z = 0$ and the size is $L_x \times L_y \times L_z = 32d_i \times 64d_i \times 16d_i$ with a spatial resolution $\Delta x = \Delta y = \Delta z = 0.05d_i \approx 3.5\lambda_{De}$, here, d_i is the ion inertia length based on n_0, λ_{De} is the electron Debye length in the current sheet. The time is normalized using the ion gyro-frequency $\Omega_i = eB/m_i$. Over 2.6×10^{10} particles for each species are used in our simulations. An initial perturbation on the magnetic field is introduced to trigger the reconnection. The perturbation is centered at $(x, y, z) = (16d_i, 0, 0)$, the edge of the simulation box, and spatially localized in the y direction with a length $L_{pert} = 20d_i$. In the x and y direction, we use periodic boundary conditions, while in the z direction, conducting boundary conditions are used for electromagnetic field, reflecting boundary conditions are used for particles.

3. Simulation Results

Figure 1 shows the time evolution of the primary reconnection. The primary reconnection x-line is introduced at the x boundary. Due to the periodic boundary conditions, the results shown here are similar to what occurs between two neighbor reconnection x-lines. The top panels show the reconnected magnetic field B_z on the $x - y$ plane, and the bottom panels show the out-of-plane current density J_y on the $x - z$ planes located at the horizontal lines plotted on the top panels, respectively. After reconnection occurs, the reconnected magnetic field B_z is gradually enhanced, forming two flux pileup regions. Near the two boundaries in the x direction, there is a thin current sheet extending along the upper-left to lower-right direction (Figure 1d), corresponding to the separatrices of the primary x-line. Later, the two flux pileup regions move toward $x = 0$ in the x direction (Figures 1e and 1f), and finally squeeze each other at $\Omega_i t = 45$, forming a current sheet extending along the z direction (Figures 1g and 1h).

We note that in Figure 1, B_z varies from positive to negative from $-x$ to $+x$ direction, such kind of bipolar B_z structure was usually identified as a flux rope, or magnetic island in 2D conditions. However, in our simulation, where the primary reconnection x-lines are short in the y direction, the bipolar B_z structure corresponds to a pair of interlinked flux tubes, rather than a flux rope. Figure 2f shows the 3D magnetic field lines and the current density J_y at $\Omega_i t = 45$, where the color of the magnetic field lines represents the amplitude of B_z. We find that the

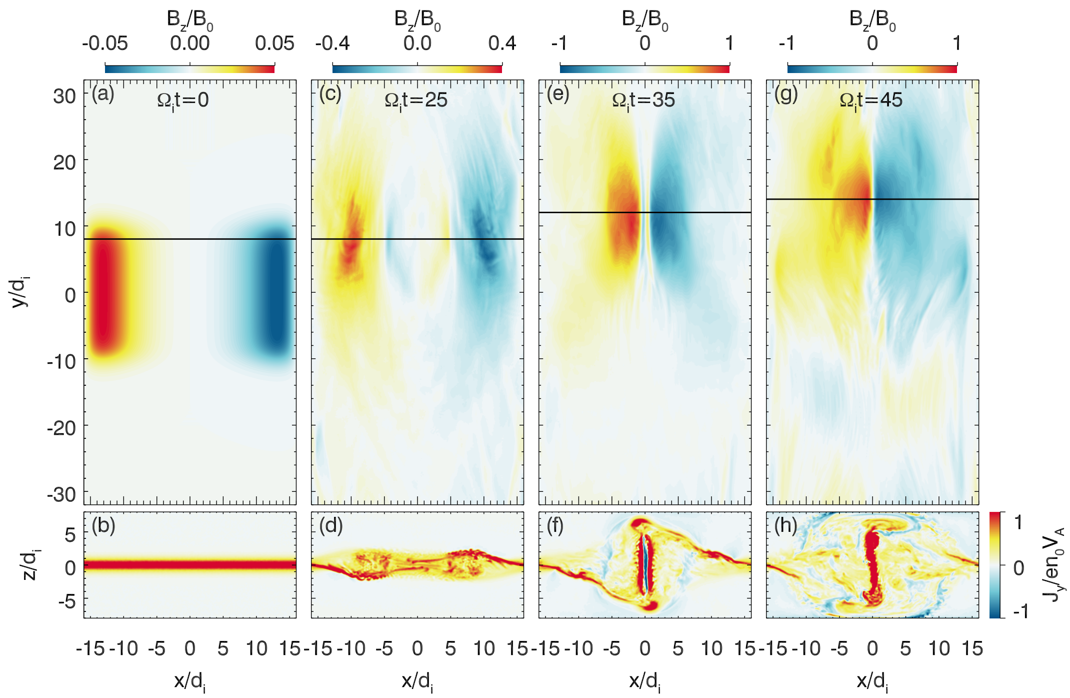

Figure 1. The top panels show the reconnected magnetic field B_z on the $z = 0$ plane at $\Omega_i t = 0$, 25, 35, and 45, respectively. The bottom panels show the current density J_y on the $x - z$ planes located at the horizontal lines plotted in the corresponding top panels.

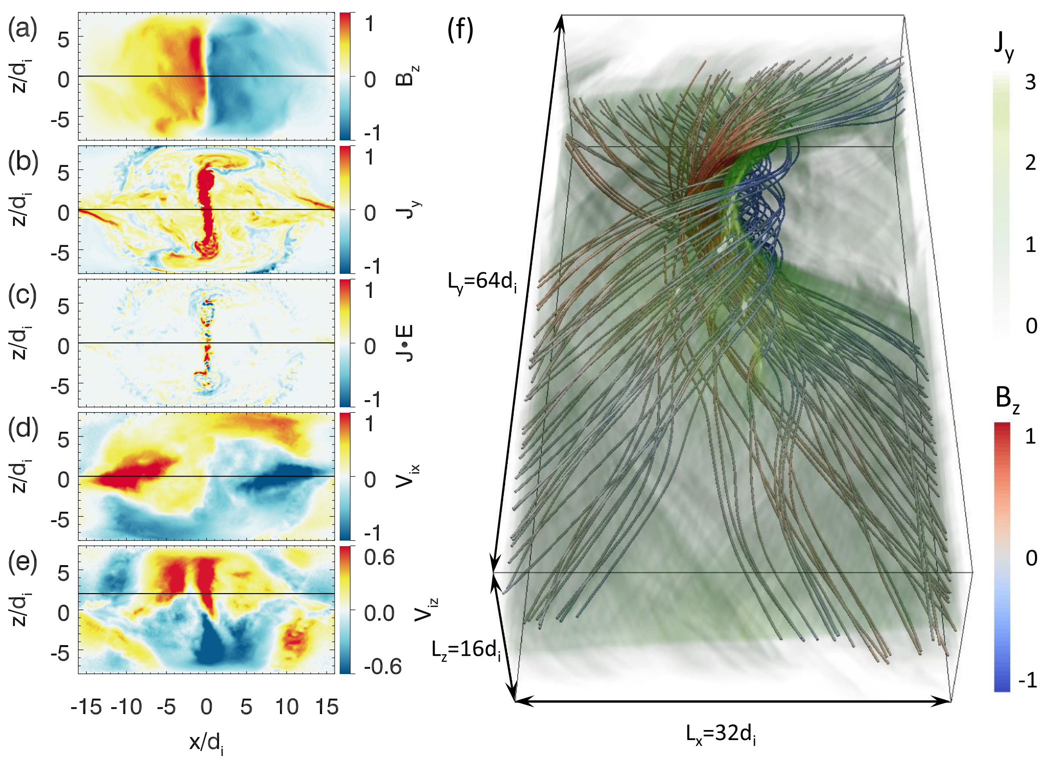

Figure 2. (a) Magnetic field B_z, (b) current density J_y, (c) energy conversion rate $J \cdot E$, (d) ion flow velocity V_{ix}, and (e) ion flow velocity V_{iz} on $y = 14d_i$ plane at $\Omega_i t = 45$. Panel (f) shows the 3D magnetic field lines with the color representing the amplitude of B_z and the contour of the current density J_y at $\Omega_i t = 45$.

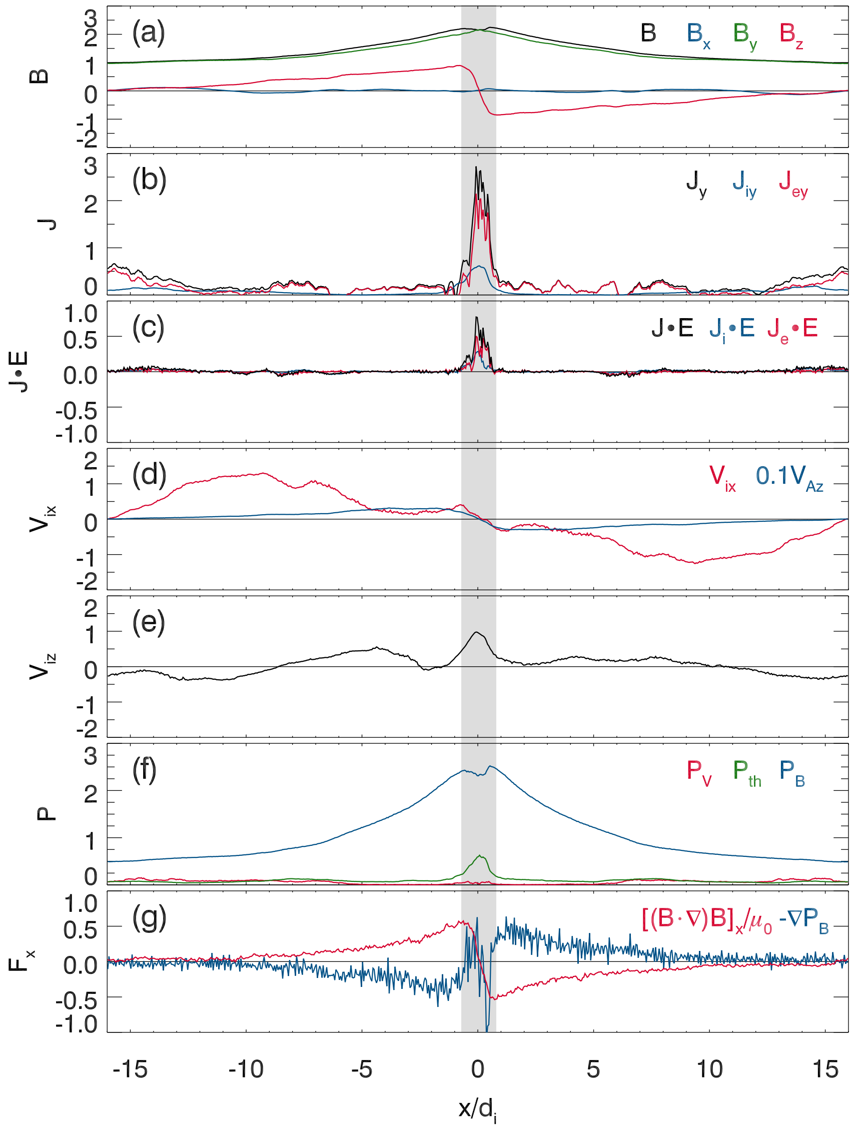

Figure 3. Panels (a–e) plot the line profiles of the quantities in Figures 2a–2e along the horizontal lines plotted in the corresponding panels in Figure 2. The blue line in panel (d) show $0.1V_{Az}$ where the local V_{Az} is defined by $V_{Az} = B_z/\sqrt{\mu_0 n m_i}$. Panel (f) plots the magnetic, thermal, and dynamic pressures. Panel (g) plots the magnetic tension force and the gradient of magnetic pressure in the x direction. Both panels (f) and (g) are plotted along $z = 0$ and $y = 14d_i$.

magnetic field lines on the two sides of the current sheet form two elbowlike flux tubes which hook each other. There is no magnetic connectivity between the two flux tubes (i.e., no helical magnetic structure as in a flux rope is formed). In panels (a-e) of Figure 2, we plot the detailed characteristics of the current sheet formed between the two interlinked flux tubes. The bipolar B_z structure in Figure 2a corresponds to the two interlinked flux tubes, and a thin current sheet is formed in between (see Figure 2b). This current sheet is ideal for the onset of secondary magnetic reconnection. In Figure 2c, we find large amplitude energy conversion rate $J \cdot E$ inside the current sheet, and there is a net positive $J \cdot E$ in the region around $-2 < z/d_i < 0$. Figures 2d and 2e show the ion flow velocity, V_{ix} presents converging flows toward the vertical current sheet, while V_{iz} shows diverging flows, consistent with the convection pattern of reconnection inflow and outflow.

Figure 3 shows the reconnection signatures inside the current sheet between the two interlinked flux tubes, the quantities in panels (a-e) are plotted along the horizontal lines shown in Figures 2a–2e) respectively. The reconnecting current sheet is highlighted using the Gy bar Figure 3a shows the three components and the amplitude of the magnetic field. At around $x = 0$, B_z reverses sign from positive to negative. The peak amplitude

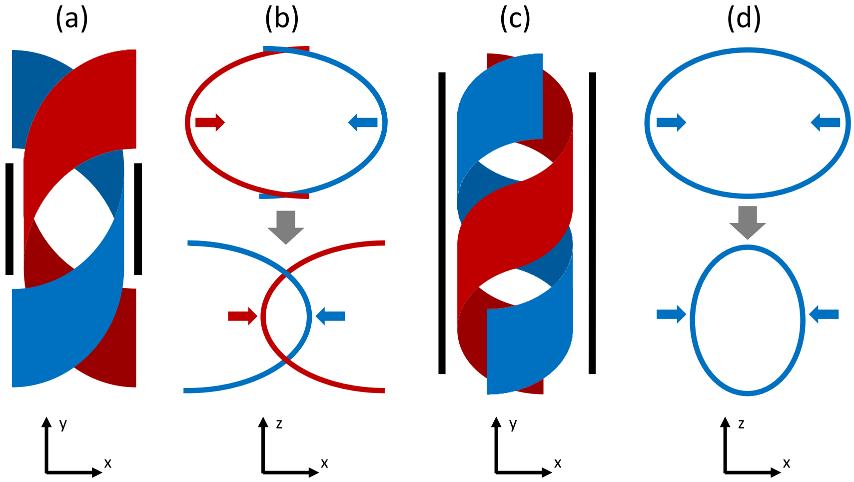

Figure 4. A cartoon sketch showing the formation of interlinked flux tubes (panels a and b) and a flux rope (panels c and d) during multiple x-line guide field reconnection.

of B_z is around $0.9B_0$, and both the amplitudes of B_y and B reach the maximum. There is a small dip in the profile of B, which is similar to the crater-shaped distribution observed by Li et al. (2023). Figure 3b shows the current density J_y, and it is mainly carried by electrons. The thickness of the current sheet is around $5d_{e,l}$ based on the local electron density $n_{e,l} \approx 0.5n_0$ (not shown). Figure 3c shows the energy conversion rate $J \cdot E$, which is positive and dominated by $J_e \cdot E$, indicating that magnetic energy is mainly converted to electrons. Figure 3d plots the ion flow velocity V_{ix} and $0.1V_{Az}$. V_{Az} is the local Alfven speed calculated by $V_{Az} = B_z/\sqrt{\mu_0 n m_i}$. V_{ix} shows converging flows on the two sides of the current sheet, and the amplitude is comparable with $0.1V_{Az}$, indicating a reconnection inflow with a reconnection rate around 0.1. Figure 3e shows the ion flow velocity V_{iz}, which is plotted along the horizontal line cross the upper outflow region (see Figure 2e). An Alfvenic ion outflow jet is observed inside the current sheet. All these features, which are similar to the observations by Øieroset et al. (2019), suggest the proceeding of magnetic reconnection inside the current sheet between the interlinked flux tubes.

In Figure 3a, we also find that the amplitude of B_z is enhanced toward the current sheet at $x = 0$, indicating strong pileup of the upstream magnetic field during reconnection. This is a typical feature for reconnection events between interlinked flux tubes in observations (Maheshwari et al., 2022). The B_z pileup was explained to overcome the suppression of magnetic reconnection due to the diamagnetic drift under the pre-pileup condition when the plasma beta β on the two sides of the current sheet is different (Maheshwari et al., 2022; Swisdak et al., 2003; Øieroset et al., 2019). Because the flux pileup leads to a lower plasma beta β, therefore the post-pileup condition is in favor of the development of reconnection. However, in our simulation, the plasma beta β on the two sides of the current sheet is symmetric, which means that this explanation for the B_z pileup does not apply to our case. In Figure 3f, we plot the profile of magnetic, thermal, and dynamic pressures along $z = 0$, the magnetic pressure reaches a maximum around $x = 0$. The thermal and dynamic pressures are much smaller than the magnetic pressure, indicating that the increase of the magnetic pressure cannot be explained by the compression by the converging flows. In Figure 3g, we plot the magnetic tension force and the gradient of magnetic pressure along the x direction. We find that the tension force has large amplitude and points toward the current sheet, balancing the gradient of magnetic pressure, consistent with the estimation by Øieroset et al. (2019). This result suggests that the pileup of the upstream magnetic field in our simulation is driven by the magnetic tension force. This situation is similar to the formation of reconnection fronts in the reconnection outflow regions (Fu et al., 2019; K. Huang et al., 2021; Sitnov et al., 2009).

In Figure 4, we use a cartoon sketch to explain why interlinked flux tubes and secondary reconnection between them can form during guide field reconnection when the x-line is short enough. Figures 4a and 4b show the condition of primary reconnection with short x-lines, while Figures 4c and 4d show the condition with long x-lines. The figures are shown in the same coordinate as our simulation, where x is the direction of the reconnecting component of the upstream magnetic field of the primary reconnection, y is the direction of the current. z is the normal direction of the current sheet. In Figures 4a and 4c, the two black thick lines represent two primary reconnection x-lines on the $x - y$ plane. The red and blue ribbons represent the flux tubes in the outflow regions of these two reconnecting x-lines. Note that there is a guide field, the magnetic field lines do not lie on the $x - z$ plane, but also extend in the y direction. Figure 4a shows that when the newly formed flux tubes from one primary x-line connect to regions outside of the neighboring x-line, it becomes one of the interlinked flux tubes. Assuming a simplified condition, if the two neighbor primary x-lines have the same length and location in the y direction, and the distance between them is D, then, interlinked flux tubes can form if the x-line length satisfies $L_{x-line} < DB_g/B_0$. In contrast, in Figure 4c, where the primary x-line is long enough, the magnetic field lines from the outflow region of one x-line can connect with those from the other x-line, forming a typical flux rope with helical magnetic field lines (Lee et al., 1993).

These two scenarios lead to different outcomes. The two interlinked flux tubes in blue and red colors in Figures 4a and 4b can drive converging flows due to the tension force; the magnetic field frozen-in to the plasma is also convected to the central region and piled up. Because there is no magnetic connection between the two interlinked flux tubes, the curvature of the magnetic field lines does not need to decrease during the convection of the field lines, as shown in Figure 4b. This process is similar to the colliding of two reconnecting fronts; the two interlinked flux tubes can continuously compress each other, forming a current sheet and secondary reconnection between them. On the other hand, in Figure 4d, during the contracting of the flux rope, the magnetic field lines only become round, and then the contraction is slowed down, preventing the formation of a thin current sheet.

4. Conclusions and Discussion

In this letter, we perform a 3D PIC simulation to study the formation of secondary reconnection between interlinked flux tubes driven by neighboring short x-lines of guide field reconnection. The characteristics of the reconnecting current sheet in our simulation agree well with observations. The pileup of the reconnecting magnetic field is attributed to the driving of the magnetic tension force. We also explain the formation condition of interlinked flux tubes versus flux ropes during multiple x-line reconnection. We estimate that the x-line should be shorter than around $L_{x-line} = DB_g/B_0$ for the system to develop interlinked flux tubes and secondary reconnection between them, it is related to the distance between two neighbor x-lines and the magnetic shear angle of the primary reconnection.

The interlinked flux tubes in our simulation show a bipolar magnetic field B_z structure and an enhancement in the out-of-plane magnetic field B_y. This feature is quite similar with a flux rope in observations. In fact, such a kind of structure had been identified as a flux rope (Øieroset et al., 2016). A statistical study of 229 FTE-type events at Earth's magnetopause found that 43 events are interlinked flux tubes with reconnection between them, while the other 186 events are regular flux ropes (Fargette et al., 2020). Based on our simulation, these interlinked flux tubes are generated through multiple x-line reconnection with a short x-line. These statistics indicate that reconnection with a short x-line (i.e., patchy reconnection) may be a common phenomenon at magnetopause. For the interlinked flux tubes observed in Øieroset et al. (2016), the spatial scale is $\sim 100 d_i$, and the magnetic shear angle of the primary reconnection is $\sim 26°$, that means the primary x-line should be shorter than $\sim 430 d_i$, still much longer than the shortest possible active x-line length around $10 d_i$ (K. Huang et al., 2020; Liu et al., 2019). Recent observation and simulation studies found the entanglement and coalescence between two flux ropes (Guo et al., 2021; Jia et al., 2021; Russell & Qi, 2020), which have helical magnetic field lines and more complicated magnetic topologies. In our simulation, magnetic reconnection occurs between two interlinked flux tubes rather than flux ropes, as shown by the 3D magnetic field lines, there is no internal twist in the flux tubes. In the real magnetosphere environments, it is expected to observe reconnection between both flux ropes and flux tubes, because the plasma conditions and magnetic geometries are much more complicated. All these studies show that magnetic reconnection plays an important role during the interaction of different magnetic structures in varieties of scenarios.

It is believed that the evolution of 3D reconnection is dominated by the formation and interaction of flux ropes (Daughton et al., 2011). Secondary reconnection can be triggered not only between two flux ropes, but also inside a single flux rope through interchange instability and Kelvin-Helmholtz instability (C. Huang et al., 2017; Lapenta et al., 2015; Lu et al., 2023; S Wang et al., 2020), and has a considerable contribution on the energy dissipation during reconnection (Lu et al., 2023). Here, we show that localized reconnection sites with short x-line is critical to the formation of interlinked flux tubes. The magnetic energy stored in these flux tubes can be further dissipated through secondary reconnection between them. This result provides a new avenue for energy dissipation during 3D magnetic reconnection.

Data Availability Statement

The simulation is performed using VPIC version 1.1. We use IDL version 8.2 and Paraview version 4.4.0 to analyze the simulation data. The simulation code, data, and scripts used to plot the figures are available at National Space Science Data Center, National Science and Technology Infrastructure of China via K. Huang (2024).

Acknowledgments
This work was supported by the NSFC Grant 42204157, and the National Key Research and Development Program of China (2022YFA1604600).

References

Angelopoulos, V., McFadden, J. P., Larson, D., Carlson, C. W., Mende, S. B., Frey, H., et al. (2008). Tail reconnection triggering substorm onset. *Science*, *321*(5891), 931–935. https://doi.org/10.1126/science.1160495

Bowers, K. J., Albright, B. J., Bergen, B., Yin, L., Barker, K. J., & Kerbyson, D. J. (2008). 0.374 Pflop/s trillion-particle kinetic modeling of laser plasma interaction on roadrunner. In *SC '08: Proceedings of the 2008 ACM/IEEE conference on supercomputing* (pp. 1–11). IEEE. https://doi.org/10.1109/sc.2008.5222734

Bowers, K. J., Albright, B. J., Yin, L., Bergen, B., & Kwan, T. J. T. (2008). Ultrahigh performance three-dimensional electromagnetic relativistic kinetic plasma simulation. *Physics of Plasmas*, *15*(5). https://doi.org/10.1063/1.2840133

Bowers, K. J., Albright, B. J., Yin, L., Daughton, W., Roytershteyn, V., Bergen, B., & Kwan, T. J. T. (2009). Advances in petascale kinetic plasma simulation with VPIC and Roadrunner. *Journal of Physics: Conference Series*, *180*, 012055. https://doi.org/10.1088/1742-6596/180/1/012055

Cardoso, F. R., Gonzalez, W. D., Sibeck, D. G., Kuznetsova, M., & Koga, D. (2013). Magnetopause reconnection and interlinked flux tubes. *Annales Geophysicae*, *31*(10), 1853–1866. https://doi.org/10.5194/angeo-31-1853-2013

Chen, G., Huang, C., Zhang, Y., Ge, Y., Du, A., Wang, R., et al. (2023). MAVEN observations of the interloop magnetic reconnections at Mars. *The Astrophysical Journal*, *952*(1), 37. https://doi.org/10.3847/1538-4357/acda90

Daughton, W., Roytershteyn, V., Karimabadi, H., Yin, L., Albright, B. J., Bergen, B., & Bowers, K. J. (2011). Role of electron physics in the development of turbulent magnetic reconnection in collisionless plasmas. *Nature Physics*, *7*(7), 539–542. https://doi.org/10.1038/nphys1965

Daughton, W., Scudder, J., & Karimabadi, H. (2006). Fully kinetic simulations of undriven magnetic reconnection with open boundary conditions. *Physics of Plasmas*, *13*(7). https://doi.org/10.1063/1.2218817

Drake, J. F., Swisdak, M., Schoeffler, K. M., Rogers, B. N., & Kobayashi, S. (2006). Formation of secondary islands during magnetic reconnection. *Geophysical Research Letters*, *33*(13). https://doi.org/10.1029/2006gl025957

Fargette, N., Lavraud, B., Øieroset, M., Phan, T. D., Toledo-Redondo, S., Kieokaew, R., et al. (2020). On the Ubiquity of magnetic reconnection inside flux transfer event-like structures at the Earth's magnetopause. *Geophysical Research Letters*, *47*(6). https://doi.org/10.1029/2019gl086726

Farinas Perez, G., Cardoso, F. R., Sibeck, D., Gonzalez, W. D., Facskó, G., Coxon, J. C., & Pembroke, A. D. (2018). Generation mechanism for interlinked flux tubes on the magnetopause. *Journal of Geophysical Research: Space Physics*, *123*(2), 1337–1355. https://doi.org/10.1002/2017ja024664

Fermo, R. L., Drake, J. F., & Swisdak, M. (2012). Secondary magnetic islands generated by the Kelvin-Helmholtz instability in a reconnecting current sheet. *Physical Review Letters*, *108*(25), 255005. https://doi.org/10.1103/PhysRevLett.108.255005

Fu, H., Grigorenko, E. E., Gabrielse, C., Liu, C., Lu, S., Hwang, K. J., et al. (2019). Magnetotail dipolarization fronts and particle acceleration: A review. *Science China Earth Sciences*, *63*(2), 235–256. https://doi.org/10.1007/s11430-019-9551-y

Guo, J., Lu, S., Lu, Q., Lin, Y., Wang, X., Huang, K., et al. (2021). Re-Reconnection processes of magnetopause flux ropes: Three-dimensional global hybrid simulations. *Journal of Geophysical Research: Space Physics*, *126*(6). https://doi.org/10.1029/2021ja029388

Hesse, M., Birn, J., & Schindler, K. (1990). On the topology of flux transfer events. *Journal of Geophysical Research*, *95*(A5), 6549–6560. https://doi.org/10.1029/JA095iA05p06549

Huang, C., Lu, Q., Guo, F., Wu, M., Du, A., & Wang, S. (2015). Magnetic islands formed due to the Kelvin-Helmholtz instability in the outflow region of collisionless magnetic reconnection. *Geophysical Research Letters*, *42*(18), 7282–7286. https://doi.org/10.1002/2015gl065690

Huang, C., Lu, Q., Wang, R., Guo, F., Wu, M., Lu, S., & Wang, S. (2017). Development of turbulent magnetic reconnection in a magnetic island. *The Astrophysical Journal*, *835*(2), 245. https://doi.org/10.3847/1538-4357/835/2/245

Huang, K. (2024). Dataset for "Secondary reconnection between interlinked flux tubes driven by magnetic reconnection with a short x-line"[DS/OL]. V2. *Science Data Bank*. https://doi.org/10.57760/sciencedb.space.01197

Huang, K., Liu, Y. H., Lu, Q., & Hesse, M. (2020). Scaling of magnetic reconnection with a limited X-line extent. *Geophysical Research Letters*, *47*(19). https://doi.org/10.1029/2020gl088147

Huang, K., Liu, Y. H., Lu, Q., Hu, Z., Lynch, K. A., Hesse, M., et al. (2022). Auroral spiral structure formation through magnetic reconnection in the auroral acceleration region. *Geophysical Research Letters*, *49*(18). https://doi.org/10.1029/2022gl100466

Huang, K., Lu, Q., Liu, Y. H., Lu, S., & Wang, R. (2023). Characteristics of magnetic reconnection with a finite X-line length. *Journal of Geophysical Research: Space Physics*, *128*(8). https://doi.org/10.1029/2022ja031209

Huang, K., Lu, Q., Lu, S., Wang, R., & Wang, S. (2021). Formation of pancake, rolling pin, and cigar distributions of energetic electrons at the dipolarization fronts (DFs) driven by magnetic reconnection: A two-dimensional particle-in-cell simulation. *Journal of Geophysical Research: Space Physics*, *126*(10). https://doi.org/10.1029/2021ja029939

Huang, S. Y., Retino, A., Phan, T. D., Daughton, W., Vaivads, A., Karimabadi, H., et al. (2016). In situ observations of flux rope at the separatrix region of magnetic reconnection. *Journal of Geophysical Research: Space Physics*, *121*(1), 205–213. https://doi.org/10.1002/2015ja021468

Jia, Y. D., Qi, Y., Lu, S., & Russell, C. T. (2021). Temporal evolution of flux rope/tube entanglement in 3-D Hall MHD simulations. *Journal of Geophysical Research: Space Physics*, *126*(3). https://doi.org/10.1029/2020ja028698

Kacem, I., Jacquey, C., Génot, V., Lavraud, B., Vernisse, Y., Marchaudon, A., et al. (2018). Magnetic reconnection at a thin current sheet separating two interlaced flux tubes at the Earth's magnetopause. *Journal of Geophysical Research: Space Physics*, *123*(3), 1779–1793. https://doi.org/10.1002/2017ja024537

Kan, J. R. (1988). A theory of patchy and intermittent reconnections for magnetospheric flux transfer events. *Journal of Geophysical Research*, *93*(A6), 5613–5623. https://doi.org/10.1029/JA093iA06p05613

Lapenta, G., Goldman, M., Newman, D. L., & Eriksson, S. (2022). Formation and reconnection of electron scale current layers in the turbulent outflows of a primary reconnection site. *The Astrophysical Journal*, *940*(2), 187. https://doi.org/10.3847/1538-4357/ac98bc

Lapenta, G., Markidis, S., Goldman, M. V., & Newman, D. L. (2015). Secondary reconnection sites in reconnection-generated flux ropes and reconnection fronts. *Nature Physics*, *11*(8), 690–695. https://doi.org/10.1038/nphys3406

Lee, L. C., Ma, Z. W., Fu, Z. F., & Otto, A. (1993). Topology of magnetic flux ropes and formation of fossil flux transfer events and boundary layer plasmas. *Journal of Geophysical Research*, *98*(A3), 3943–3951. https://doi.org/10.1029/92ja02203

Li, X., Wang, R., & Lu, Q. (2023). Division of magnetic flux rope via magnetic reconnection observed in the magnetotail. *Geophysical Research Letters*, *50*(1). https://doi.org/10.1029/2022gl101084

Liu, Y. H., Li, T. C., Hesse, M., Sun, W. J., Liu, J., Burch, J., et al. (2019). Three-dimensional magnetic reconnection with a spatially confined X-line extent: Implications for dipolarizing flux bundles and the dawn-dusk asymmetry. *Journal of Geophysical Research: Space Physics*, *124*(4), 2819–2830. https://doi.org/10.1029/2019ja026539

Louarn, P., Fedorov, A., Budnik, E., Fruit, G., Sauvaud, J. A., Harvey, C. C., et al. (2004). Cluster observations of complex 3D magnetic structures at the magnetopause. *Geophysical Research Letters*, *31*(19). https://doi.org/10.1029/2004gl020625

Lu, Q., Fu, H., Wang, R., & Lu, S. (2022). Collisionless magnetic reconnection in the magnetosphere. *Chinese Physics B*, *31*(8), 089401. https://doi.org/10.1088/1674-1056/ac76ab

Lu, Q., Huang, K., Guan, Y., Lu, S., & Wang, R. (2023). Energy dissipation in magnetic islands formed during magnetic reconnection. *The Astrophysical Journal*, *954*(2), 146. https://doi.org/10.3847/1538-4357/acea86

Maheshwari, K., Phan, T. D., Øieroset, M., Fargette, N., Lavraud, B., Burch, J. L., et al. (2022). Investigation of the diamagnetic drift condition for the suppression of magnetic reconnection in 3D interlinked reconnection events with magnetic flux pileup. *The Astrophysical Journal*, *940*(2), 177. https://doi.org/10.3847/1538-4357/ac9405

Masuda, S., Kosugi, T., Hara, H., & Ogawara, Y. (1994). A loop top hard X-ray source in a compact solar-flare as evidence for magnetic reconnection. *Nature*, *371*(6497), 495–497. https://doi.org/10.1038/371495a0

Nishida, A. (1989). Can random reconnection on the magnetopause produce the low latitude boundary-layer. *Geophysical Research Letters*, *16*(3), 227–230. https://doi.org/10.1029/GL016i003p00227

Øieroset, M., Phan, T. D., Drake, J. F., Eastwood, J. P., Fuselier, S. A., Strangeway, R. J., et al. (2019). Reconnection with magnetic flux pileup at the interface of converging jets at the magnetopause. *Geophysical Research Letters*, *46*(4), 1937–1946. https://doi.org/10.1029/2018gl080994

Øieroset, M., Phan, T. D., Haggerty, C., Shay, M. A., Eastwood, J. P., Gershman, D. J., et al. (2016). MMS observations of large guide field symmetric reconnection between colliding reconnection jets at the center of a magnetic flux rope at the magnetopause. *Geophysical Research Letters*, *43*(11), 5536–5544. https://doi.org/10.1002/2016gl069166

Otto, A. (1995). Forced three-dimensional magnetic reconnection due to linkage of magnetic flux tubes. *Journal of Geophysical Research*, *100*(A7), 11863–11874. https://doi.org/10.1029/94ja03341

Russell, C. T., & Elphic, R. C. (1978). Initial ISEE magnetometer results: Magnetopause observations. *Space Science Reviews*, *22*(6). https://doi.org/10.1007/bf00212619

Russell, C. T., & Qi, Y. (2020). Flux ropes are born in pairs: An outcome of interlinked, reconnecting flux tubes. *Geophysical Research Letters*, *47*(15). https://doi.org/10.1029/2020gl087620

Sergeev, V. A., Angelopoulos, V., & Nakamura, R. (2012). Recent advances in understanding substorm dynamics. *Geophysical Research Letters*, *39*(5). https://doi.org/10.1029/2012gl050859

Shibata, K., Masuda, S., Shimojo, M., Hara, H., Yokoyama, T., Tsuneta, S., et al. (1995). Hot-plasma ejections associated with compact-loop solar-flares. *The Astrophysical Journal*, *451*(2), L83. https://doi.org/10.1086/309688

Sitnov, M. I., Swisdak, M., & Divin, A. V. (2009). Dipolarization fronts as a signature of transient reconnection in the magnetotail. *Journal of Geophysical Research*, *114*(A4). https://doi.org/10.1029/2008ja013980

Swisdak, M., Rogers, B. N., Drake, J. F., & Shay, M. A. (2003). Diamagnetic suppression of component magnetic reconnection at the magnetopause. *Journal of Geophysical Research*, *108*(A5). https://doi.org/10.1029/2002ja009726

Wang, L., Huang, C., Du, A., Ge, Y., Chen, G., Yang, Z., et al. (2023). Kelvin–helmholtz instability at mars: In situ observations and kinetic simulations. *The Astrophysical Journal*, *947*(2), 51. https://doi.org/10.3847/1538-4357/acc655

Wang, L., Huang, C., Ge, Y., Du, A., Wang, R., Zhang, T., et al. (2022). Heavy ion escape from martian wake enhanced by magnetic reconnection. *Journal of Geophysical Research: Planets*, *127*(6). https://doi.org/10.1029/2022je007181

Wang, R., Lu, Q., Du, A., & Wang, S. (2010). In SituObservations of a secondary magnetic island in an ion diffusion region and associated energetic electrons. *Physical Review Letters*, *104*(17), 175003. https://doi.org/10.1103/PhysRevLett.104.175003

Wang, R., Lu, Q., Nakamura, R., Huang, C., Du, A., Guo, F., et al. (2015). Coalescence of magnetic flux ropes in the ion diffusion region of magnetic reconnection. *Nature Physics*, *12*(3), 263–267. https://doi.org/10.1038/nphys3578

Wang, S., Wang, R., Lu, Q., Fu, H., & Wang, S. (2020). Direct evidence of secondary reconnection inside filamentary currents of magnetic flux ropes during magnetic reconnection. *Nature Communications*, *11*(1), 3964. https://doi.org/10.1038/s41467-020-17803-3

Zhang, T. L., Lu, Q. M., Baumjohann, W., Russell, C. T., Fedorov, A., Barabash, S., et al. (2012). Magnetic reconnection in the near venusian magnetotail. *Science*, *336*(6081), 567–570. https://doi.org/10.1126/science.1217013

Zhong, Z. H., Tang, R., Zhou, M., Deng, X., Pang, Y., Paterson, W., et al. (2018). Evidence for secondary flux rope generated by the electron Kelvin-Helmholtz instability in a magnetic reconnection diffusion region. *Physical Review Letters*, *120*(7), 075101. https://doi.org/10.1103/PhysRevLett.120.075101